Acta Materialia 105 (2016) 25–34

Contents lists available at ScienceDirect

Acta Materialia

journal homepage: www.elsevier.com/locate/actamat

Full length article

Anomalous evolution of microstructure and crystallographic texture during indentation

Saurabh Basu, Zhiyu Wang, Christopher Saldana*

George W. Woodruff School of Mechanical Engineering, Georgia Institute of Technology, 801 Ferst Drive, Atlanta, GA, USA

ARTICLE INFO

Article history:
Received 2 October 2015
Received in revised form
5 December 2015
Accepted 13 December 2015
Available online xxx

Keywords:
Indentation
Microstructure
Texture

ABSTRACT

The present work combines orientation imaging microscopy (OIM) and visco-plastic self-consistent framework based numerical simulation to study evolution of microstructure and crystallographic texture during indentation of copper. It was seen that anomalous microstructure evolution characteristics involving accelerated grain fragmentation and refinement resulted in ultra-fine grains at low equivalent strains within a zone close to the interface of the indenter. Sources of acceleration in refinement were found in enhanced local crystallographic rotation rates manifesting through micro-scale strain-path changes in pathlines leading into the zone near the interface. These strain path changes were shown to result from heterogeneous accommodation of deformation across mechanically harder/softer micro-zones prevalent in copper despite absence of a harder second phase. The micro-zones were recognized using Taylor factor analysis by coupling in-situ characterization of deformation fields with OIM. In addition to accelerated refinement, zones near the interface of the indenter also exhibited cube textures as opposed to shear-type textures elsewhere in the specimen, confirming a hitherto unknown heterogeneity in the geometry of deformation mechanics imposed during indentation.

1. Introduction

Ease of sample preparation and high throughput make indentation a powerful tool for mapping constitutive behavior of metals [1] and characterization of an array of material parameters such as residual stresses [2], stress–strain relationships [1], scale dependence of material response [3] and critical resolved shear stress [4]. These parameters are extracted from force (P) vs. indentation depth (h) curves representative of the material's mechanical behavior, sometimes supplemented with additional post-mortem characterization [5]. The mechanical behavior of materials during indentation is complicated by heterogeneous deformation [6,7], orientation dependence of material flow [8–10], anisotropy of yield surfaces [11] and friction effects [12] that render force (P) vs. indentation depth (h) curves equivocal. The influence of these effects complicates characterization of constitutive behavior as a function of fundamental material parameters. This can be mitigated with a complete understanding of plastic flow during indentation, whereby individual contributions from the aforementioned effects to the resulting P *vs.* h curves can be quantified. A parameter that has been shown to play a profound role on the plastic response of metallic materials is crystallographic texture [13]. Presence of textures constituting high concentrations of preferred orientations is known to influence formability by governing the onset of shear banding [14–16], anisotropy in polycrystal yield strengths [17] and stress–strain relations [18]. Predicting behavior in the presence of crystallographic textures often necessitates modeling their evolution during plastic deformation which can be done using the visco plastic self consistent (VPSC) framework [19] coupled with image correlation techniques or finite element methods (FEM) explicitly [20] or implicitly [21].

Preferred crystallographic textures in polycrystals originate as a consequence of thermomechanical history imposed by plastic deformation [13,22], this concomitantly influencing evolution of microstructure [23,24]. For instance, deformation involving strain histories constituting strain path changes and interfering crystallographic textures are known to result in accelerated microstructure refinement. This phenomena has been seen in the C route of equal channel angular pressing (ECAP), which involves globally-imposed strain path changes. After two passes with $\varepsilon \sim 2$, the C route results in a smaller final grain size compared with rolling to $\varepsilon \sim 2$, the latter featuring a monotonic strain history [23]. Similar

* Corresponding author.
E-mail address: christopher.saldana@me.gatech.edu (C. Saldana).

http://dx.doi.org/10.1016/j.actamat.2015.12.028
1359-6454/

variation has also been seen for different ECAP routes. For instance, the *B* route has been recognized to result in faster grain refinement with more -ve $\frac{\partial \delta}{\partial \varepsilon}$ where δ is the grain size, than other routes during ECAP of pure Al [25] due to global changes in direction of imposed shear. Presumably, the evolution of microstructures and crystallographic textures during indentation also follows complex routes due to heterogeneity in imposed plastic strains [6,7]. Additionally, material trajectories in the deformation zone of indentation can be expected to traverse through spatially-varying stress fields, wherein micro-scale strain path changes may be imposed. While strain histories of material points have been studied during indentation, characterization of strain path changes and their influence on material response during indentation have not been well addressed. In this study, evolution of microstructures and crystallographic textures during circular indentation is investigated. It is shown that the zone closest to the interface of the indenter within the workpiece experiences spatial strain-gradients and strain path changes that contribute significantly to anomalous microstructure and texture evolution within this zone.

2. Experimental methods

Circular indentation, diameter $d = 1\ mm$, was performed on annealed oxygen free high conductivity copper (OFHC Cu) featuring a mean grain size ~50 μm. A two-dimensional plane strain indentation configuration was imposed by setting $t \gg d$ in order to avail characterization of material flow using digital image correlation (DIC), where Fig. 1(a) identifies dimensions t and d. The depth of indentation h_{max} was limited to 0.5 mm and the speed of indentation v was set at 0.1 $mm\ s^{-1}$ in order to avoid temperature rise due to heat dissipated during plastic deformation.

Characterization of deformation flow fields during indentation was performed by DIC of recorded images of material flow using a PCO DIMAX camera equipped with a Navitar ZOOM 6000 optical lens assembly, this yielding an optical resolution ~3 μm/pixel. Digital images furnish exact spatial locations of asperities on the surface of the sample during the deformation experiment. Using an image correlation algorithm, the motions of asperities due to the imposed deformation was thereafter quantified. This involved calculation of the normalized cross-correlation coefficient given by Refs. [26,27]: $\Phi_k(m,n) = \sum_{j=1}^{q}\sum_{i=1}^{p} f_k(i,j) f_{k+1}(i+m, j+n)$. Here, $f_k(i,j)$ and $f_{k+1}(i+m, j+n)$ refer to intensities at locations (i,j) and $(i+m, j+n)$ in digital images f_k and f_{k+1} in the sequence, respectively. The global maxima in the cross correlation function identifies the location of the asperity $(i+m, j+n)$ in image f_{k+1} whose original location in image f_k was (i,j). In this manner, displacement undergone by an asperity at (i,j) in image f_k given by (m,n) was found. Sub pixel ($\frac{1}{10}th$ pixel) accuracy was achieved using linear intra-pixel interpolation. Thereafter, the displacement vector field in the region of interest (ROI) captured by digital imaging was constituted and subsequently differentiated spatially and temporally to produce velocity gradient $L_{ij} = \frac{\partial v_i}{\partial x_j}$ and strain rate $\dot{\varepsilon}_p = \frac{1}{2}(\underline{L} + \underline{L}^T)$ tensor fields. To produce effective strain fields, pathlines followed by asperities in the ROI were quantified. Subsequently, effective strain fields were calculated using a path integral, given by $\varepsilon(x,y) = \oint \sqrt{\frac{2}{3}\underline{\dot{\varepsilon}_p} : \underline{\dot{\varepsilon}_p}}\, dt$, where : refers to the inner product. In addition, Lagrangian strain tensor fields were calculated in order to identify anisotropy in imposed global strains and material response. This was done by calculating the deformation gradient tensor field using $\underline{L} = \underline{\dot{F}} \cdot \underline{F}^{-1}$ and subsequently using $\underline{E}^{pl} = \frac{1}{2}(\underline{F}^T \cdot \underline{F} - \underline{I})$ where $\underline{I}$ is the identity tensor.

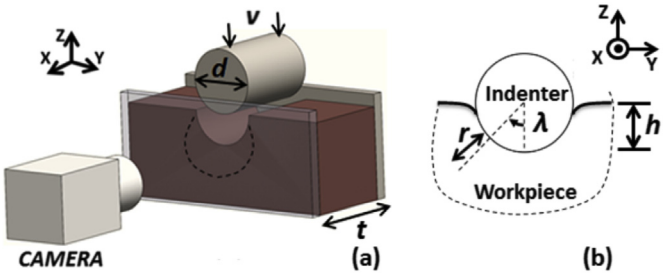

Fig. 1. (a) Three dimensional schematic of the circular indentation setup used for performing digital image correlation. (b) Schematic of circular indentation setup for identifying material characterization parameters ($r(\mu m)$,$\lambda(deg)$).

Quantitative orientation imaging microscopy (OIM) of pre- and post-indentation workpieces was performed using electron backscattered diffraction (EBSD) in a Tescan Mira 3 thermal field emission scanning electron microscope equipped with a EDAX TSL EBSD detector. Sample preparation involved mechanical polishing to a 0.05 μm surface finish followed by ion polishing in a Hitachi 4000 plus ion beam polisher for ~300 s. Scan step sizes <0.2 μm were employed. Crystallographic textures were extracted from OIM data using the freely available MATLAB-based software MTEX [28].

Evolution of crystallographic textures in the deformation zone was numerically simulated using a FORTRAN implementation of the VPSC framework [29]. VPSC is a numerical approximation of material response that implicitly simulates evolution of grain morphologies and crystallographic textures due to imposed plastic deformation. To this end, the framework relies on deformation history within the ROI, which was obtained from DIC-based characterization of material flow. To this end, deformation histories of pathlines within the ROI were compiled as velocity gradient tensors $L_{ij} = \frac{\partial v_i}{\partial x_j}$ through the deformation imposed during indentation. VPSC also utilizes pre-deformation crystallographic texture as discrete orientation distribution functions (ODF), representative of the pristine state of the workpiece undergoing plastic deformation. Herein, a uniformly distributed list of 5000 orientations was produced using MATLAB. Post-deformation crystallographic textures were compared with empirical counterparts obtained from OIM. This was done by calculating: $\widehat{T}^d = \frac{\int [f_{sim}(g) - f_{exp}(g)]^2 dg}{\int f_{exp}(g)^2 dg}$, where g refers to orientation.

3. Results

3.1. In-situ characterization of deformation fields

Strain fields were characterized within a region close to the indenter, demarcated using a white box in Fig. 2(a). Spatially heterogeneous effective and Lagrangian strain fields developed under the indenter, reminiscent of deformation fields seen during flat punch indentation [6]. Material directly underneath the indenter at $(r,\lambda) = (r,0^\circ)$ with $r < 20\ \mu m$ exhibited a local minima in ε, where Fig. 1(b) defines the polar coordinate system (r,λ). This region was surrounded by a zone that featured higher ε, in the vicinity of the dashed line identified in Fig. 2(b). The intersecting location between the dashed line and the interface of the indenter at $(r,\lambda) = (0\mu m, +45^\circ)$ exhibited global maxima in effective strains: $\varepsilon_{max} = 4.5$. Locations that developed maxima and minima are identified with black and white arrows, respectively, in Fig. 2(b). Effective strains decayed to negligible levels at greater r.

Evolution of Lagrangian strain tensor components with respect to indentation depth h is shown in Fig. 3 for different locations underneath the indenter. Directly underneath the interface at $(r,\lambda) = (r,0^\circ)$, where $r > 0\ \mu m$, the strain histories generally featured greater shear magnitudes relative to that of tensile/compressive components. This is shown in Fig. 3(a) in curves *i*, *ii*, *iii* and *iv* for $(r,\lambda) = (45\ \mu m, 0^\circ)$, $(51\ \mu m, 0^\circ)$, $(57\ \mu m, 0^\circ)$ and $(100\ \mu m, 0^\circ)$, these